ELSEVIER

Biochimica et Biophysica Acta 1467 (2000) 307–325

BIOCHIMICA ET BIOPHYSICA ACTA
BBA

www.elsevier.com/locate/bba

Conformational studies of sphingolipids by NMR spectroscopy. I. Dihydrosphingomyelin

Stacey R. Ferguson-Yankey [a], Douglas Borchman [b], K. Grant Taylor [a], Donald B. DuPré [a], M. Cecilia Yappert [a,b,*]

[a] *Department of Chemistry, University of Louisville, Louisville, KY 40292, USA*
[b] *Department of Ophthalmology and Visual Sciences, University of Louisville, Louisville, KY 40292, USA*

Received 5 March 1999; received in revised form 18 April 2000; accepted 20 April 2000

Abstract

The conformational features of dihydrosphingomyelin (DHSM), the major phospholipid of human lens membranes, were investigated by ^{1}H and ^{31}P nuclear magnetic resonance spectroscopy. Several postulates emerge from the observed trends: (a) in partially hydrated samples of DHSM in $CDCl_3$ above 13 mM, at which lipid–lipid interactions prevail, the amide proton is mostly involved in intermolecular H-bonds that link neighboring phospholipids through bridging water molecules. In the absence of water, the NH group is involved in an intramolecular H-bond that restricts the mobility of the phosphate group. (b) In the monomeric form of the lipid molecule, the amide proton of the major conformer is bound intramolecularly with one of the anionic and/or ester oxygens of the phosphate group. A minor conformer may also be present in which the NH proton participates in an intramolecular H-bond linking to the OH group of the sphingoid base. (c) Complete hydration leads to an extension of the head group as water molecules bind to the phosphate and NH groups via H-bonds, thus disrupting the intramolecular H-bonds prevalent at low concentrations.

Keywords: Dihydrosphingomyelin; Human lens phospholipid; H-bonding; Nuclear magnetic resonance; Conformation; Lipid–lipid interaction

1. Introduction

Sphingophospholipids or sphingomyelins (SMs) are the most abundant sphingolipids in biomembranes [1,2]. The most commonly occurring sphingophospholipid in animal tissue membranes is SM whose structure was proven to be *N*-acyl-sphingosine-1-phosphorylcholine or ceramide-1-phosphorylcholine in 1927 [3]. The sphingoid base in SM is sphingosine, an 18-carbon amine diol: 1,3-dihydroxy-2-amino-4-octadecene, whose enantiomeric configuration is D-*erythro*, as the chiral carbons 2 and 3, to which OH and NH_2 groups attach, respectively, are in the 2*S*,3*R* configuration [4]. The *trans* double bond is located between carbons 4 and 5 of sphingosine [4]. Until recently, only very small amounts of the saturated base 1,3-dihydroxy-2-amino-octadecane, also known as dihydrosphingosine or sphinganine, had been reported in natural membranes [5].

The phospholipid composition of plasma membranes of human lenses is unique as these membranes

* Corresponding author. Fax: +1-502-852-8149; E-mail: mcyappert@louisville.edu

0005-2736/00/$ – see front matter
PII: S0005-2736(00)00228-5

contain a sphingolipid which is unusual in both its nature and high content. This component, mistakenly believed to be SM for several decades [6–8], was first reported as an unknown phospholipid in 1991 [9] for its ^{31}P chemical shift did not match that of any phospholipid found in other membranes. In 1994, we were able to isolate this unknown phospholipid [10] and identify it [10,11] as D-*erythro* dihydrosphingomyelin (DHSM). As shown in Fig. 1, DHSM differs from SM in that its sphingoid base, sphinganine, does not contain the double bond between carbons 4 and 5 found in SM. DHSM accounts for about 50% of the phospholipids in human lens membranes. Interestingly, and unlike SM, this unusually high amount of DHSM does not change with age and lens region [12]. Membranes of other mammalian lenses [13] and other tissues contain only minuscule amounts of DHSM [5]. Literature reports dealing with DHSM before 1994 are scarce [14–17], possibly because this lipid was thought to be a very minor component in most membranes. Until now, most of the structural characterization on sphingophospholipids has focussed on SM [18–29], and there are no reports on the structural properties and biological role(s) of DHSM. We have shown, however, that the gel to liquid crystalline phase transition temperature, T_c, of DHSM isolated from human lenses is 41°C, 9°C higher than that of SM [30]. This is indicative of stronger intermolecular associations established by DHSM in membrane organizations.

Interestingly, in the de novo synthesis of SM [31], dihydroceramide (sphinganine+fatty acid) is formed first. The double bond is then introduced to result in ceramide. The addition of the phosphorylcholine head group to ceramide represents the final step in the synthesis of SM. It appears then that this double bond may impart specific conformational features needed for the proper function of biomembranes. Another very intriguing aspect related to the biological role(s) of sphingolipids emerged in the late 1980's, when the metabolic products of SM, ceramide, sphingosinephosphorylcholine and sphingosine, were proposed to act as lipid second messengers in cell-signaling mechanisms involved in a variety of cell processes, including cell growth, differentiation and programmed cell death or apoptosis [32–37]. In several of these processes, the presence of the double bond between carbons 4 and 5 appears to be critical.

Another unusual feature of human lens membranes is the extremely high amount of cholesterol present. While most mammalian membranes exhibit a molar ratio of cholesterol to phospholipid of less than one, this ratio averages three in human lenses [38,39]. Recent studies have demonstrated the presence of lipid clusters rich in cholesterol and sphingolipids in some cell membranes [40–42]. Some of these microdomains serve as 'rafts' involved in membrane trafficking and signaling processes while others known as 'caveolae' adopt a flask-like shape and host specific proteins [40–42]. The presence of cholesterol-immiscible domains has been reported in human lens membranes [43] and we have recently isolated them from cortical and nuclear fiber membranes [44].

As we seek to unravel the structural roles of sphingolipids in human lens membranes, our first step has been to characterize the conformational features of DHSM by high-resolution nuclear magnetic resonance (NMR) spectroscopy. We began our studies by studying DHSM with different levels of hydration in chloroform. The reasons for this solvent choice are various: (a) in aqueous media, the aggregation of lipids into liposomes leads to excessive broadening of resonance bands and does not allow the observation of structural changes that take place with extensive molecular association; (b) in light of the high levels of cholesterol in human lens membranes and the possible formation of sphingolipid–cholesterol clusters, chloroform may provide a rational lens membrane mimetic environment; (c) the conformations adopted by the interface and head group regions of sphingolipids in the reverse micelles established in chloroform may approximate those in the highly curved membrane of caveolae; (d) by varying the sphingolipid concentration and the sample temperature, it is possible to observe the conformational changes that take place as the head group, interfacial and hydrophobic regions of neighboring lipids come into close proximity and lipid–lipid interactions are established and (e) by varying the level of hydration of the lipid, the role of bound water molecules in the conformational preferences of the lipids and in the formation of lipid interactions can be inferred.

2. Materials and methods

2.1. Sample preparation

DHSM was prepared from bovine brain SM (Sigma, St. Louis, MO, USA) by catalytic hydrogenation at room temperature as described previously [11]. The complete hydrogenation of SM to DHSM was confirmed by ^{31}P NMR spectroscopy. For the complete assignment of proton and ^{13}C NMR chemical shifts, two-dimensional (2D) ^{1}H–^{13}C heteronuclear multiple quantum coherence (HMQC) spectroscopy, ^{1}H-^{1}H COSY and total correlation spectroscopy (TOCSY) [45], also known as homonuclear Hartmann-Hahn or HOHAHA [46], were applied to mixtures of DHSM in $CDCl_3$.

To investigate the nature of intra- and intermolecular interactions, spectral data were acquired over a concentration range extending from 1 to 160 mM. In addition, temperature-dependent studies were carried out in DHSM samples prepared in three different pure solvents: deuterium oxide (D_2O), deuterated benzene (C_6D_6) and deuterated cyclohexane (C_6D_{12}). In the preparation of all the samples, the proper amount of DHSM, assuming a molecular weight of 780 g/mol, was weighed and the solvent was added. The molecular weight used was the median of the range of molecular weights provided by Sigma for SM. To ensure homogeneity in the samples, heating to 50°C was not enough and pulsated sonication was needed. The 5 min sonication sequence included 0.5 s pulses followed by a 1 min delay and a second pulse for 15 s. During the sonication, a minute amount of solvent may have evaporated. Therefore, the reported concentrations are not to be considered exact, as they may be slightly greater due to a small loss of solvent.

The samples prepared as indicated above were *partially hydrated*. The amount of water present in these samples was assessed by integration of the proton resonance bands corresponding to bound water molecules. The integration was four to six protons, indicative of the presence of two to three bound water molecules per phospholipid. Spectral studies were carried out to characterize the nature of lipid–water interactions using both dehydrated and fully hydrated samples. *Dehydrated samples* were prepared by removing bound water molecules with the application of a vacuum level of 10^{-2} Torr for 12 h or longer. Based on infrared spectral studies, 12 h of vacuum were sufficient to eliminate the OH stretching absorption band due to bound water molecules. This broad band is centered at ca. 3400 cm^{-1}. It is possible, however, that trace amounts of water were still present in these samples due to water impurities in the chloroform solvent. However, since the proton resonance associated with water impurities in chloroform exhibited a low chemical shift ($\delta = 1.52$ ppm) and differed from that of the bound water molecules ($\delta > 1.6$ ppm), it was possible to estimate the relative amount of bound water in the DHSM samples. For concentrations of DHSM above 13 mM, the dehydrated samples had less than one water molecule per phospholipid, as indicated by the integration of the resonance bands. Hydration studies were carried out by adding small aliquots (20 to 50 μl) of H_2O or D_2O to the partially hydrated DHSM. In these *hydrated samples*, the molar ratio of water to phospholipid was 50:1 or greater.

2.2. One-dimensional (1D) NMR studies

NMR experiments were performed on a Bruker AMX 500 spectrometer operating at a 500.1, 125.8 and 202.5 MHz for ^{1}H, ^{13}C and ^{31}P frequencies, respectively. ^{1}H NMR spectra were recorded at temperatures varying from 35 to 50°C. The ^{13}C NMR spectra were recorded only at 50°C as most resonances were severely broadened and thus hardly detectable at temperatures below 35°C. ^{31}P NMR spectra were obtained over a sweep width of 5 ppm using a 3 μs pulse width with a delay time of 1 s and an acquisition time of 1.5 s. All 1D spectra were processed using Bruker WINNMR software on a personal computer.

2.3. 2D NMR experiments

The ^{1}H–^{1}H COSY and ^{1}H–^{13}C HMQC experiments were performed with an inverse probe, while all other NMR experiments, including TOCSY were obtained using a quad probe. The HMQC spectral data were acquired with a phase sensitive mode using time-proportional phase incrementation and the bilinear rotation decoupling (BIRD) preparation pulse [47]. A total of 96 scans were collected per free in-

duction decay (FID). The ^1H–^1H COSY spectra were acquired using the parameters reported previously [10]. For both the COSY and the HOHAHA experiments, a total of eight scans were accumulated per FID. The data for all 2D spectra were recorded as 256 experiments, with 512 complex points. Sweep widths of 5 ppm for ^1H and 70 ppm for ^{13}C were used. The spectra were apodized by a 90°-shifted sinebell function and zero filled to 1024 in each dimension. The acquired data were treated on a Silicon Graphics computer using the program FELIX.

2.4. Longitudinal relaxation times, T_1, and correlation times τ_c

Experiments for the determination of proton T_1 values were performed on DHSM samples prepared in $CDCl_3$ at various concentrations and in D_2O using the Bruker 500 MHz NMR spectrometer. Sixteen scans were collected for each FID and variable delays of 32, 0.01, 0.02, 0.04, 0.08, 0.16, 0.32 and 0.64 s were used in the pulse sequence. T_1 values were determined from 37 to 50°C with the Bruker software. In a similar fashion, proton T_1 values were measured using the INOVA 300 MHz Varian spectrometer. The correlation times τ_c were estimated by approximating the rate of relaxation to the sum of the rates W_1+W_2, corresponding to the transitions with a change in the magnetic quantum number $\Delta M=1$ for W_1 and $\Delta M=2$ for W_2. These relaxation rates are related to τ_c and the applied frequency ω ($\omega=2\pi\nu$; ν=frequency of NMR spectrometer) as follows [48]: $W_1=\tau_c/(1+\omega^2\tau_c^2)$ and $W_2=4\tau_c/(1+4\omega^2\tau_c^2)$. By measuring the T_1 values at two different frequencies, 300 and 500 MHz in this case, τ_c values can be estimated [48].

3. Results

The labeling of each resonance corresponds to the atom numbering scheme used in Fig. 1. This nomenclature is a slight modification of that devised for ceramides by Pascher [21] and it simplifies the more complex scheme of Sundaralingam [49]. In addition, the proposed labeling retains the numbering scheme used for the sphingoid bases and follows the sequence of biochemical formation of sphingophospholipids [31]. The carbons of the sphingoid base carry the numbers 1, 2, 3, etc., beginning with the carbon closest to the phosphate group. The fatty acid branch, which in the de novo synthesis is added to the sphinganine before the head group, is labeled with singly primed numbers beginning with the carbon involved in the peptide bond. Finally, the choline moiety, which represents the last step in the de novo synthesis of SM [31], is labeled with doubly primed numbers beginning with the carbon closest to the phosphate group. Each atom associated with a carbon retains the number of the carbon, and in cases where there are two identical, but either chemically or magnetically nonequivalent atoms, they are differentiated by adding the letter A or B.

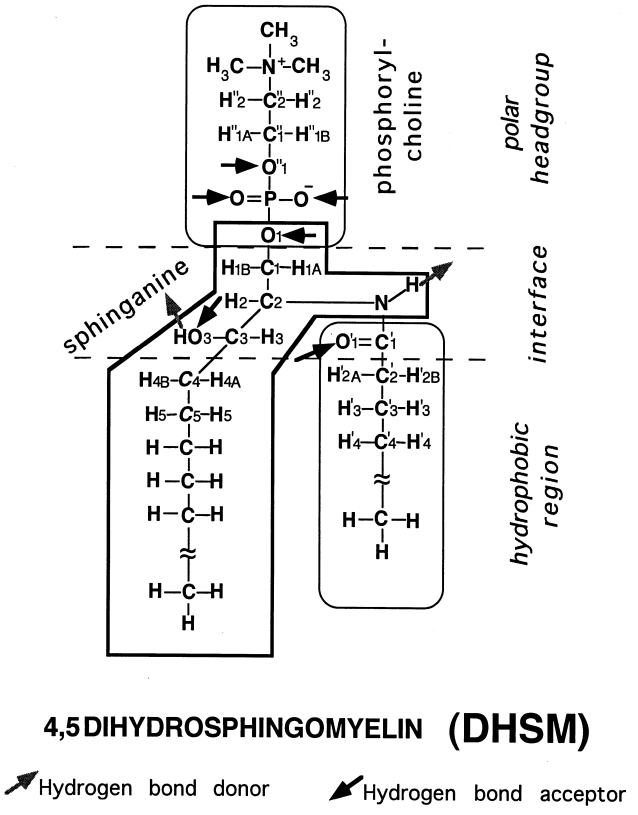

Fig. 1. Components, regions and atom numbering of DHSM.

3.1. ^1H NMR spectral assignments

The assignments of DHSM proton resonances listed in Table 1 confirm our previous reports on DHSM isolated from human lens membranes [10,11] and present more specific ones for other pro-

Table 1
Spectral assignment of ^{1}H NMR resonances observed for 80 mM DHSM in $CDCl_3$ at 50°C

Chemical shift (ppm)	Assignment	Observed shape multiplicity
0.87	CH_3 (terminal methyl) (hydrophobic chains)	triplet
1.25	CH_2 (methylene) (hydrophobic chains)	broad
1.33, 1.49	**H**4	unresolved
1.59	**H′**3	unresolved
2.16	**H′**2	broad decaplet
3.25	$N^+(CH_3)_3$	singlet
3.51	**H**3	triplet ($J \sim 7.5$ Hz)
3.69	**H″**2	singlet
3.88	**H**2	unresolved
3.96	**H**1B	unresolved
4.03	**H**1A	unresolved
4.25	**H″**1A	unresolved
	H″1B	
5.28	**OH**	very broad
7.09	**NH**	broad doublet ($J = 7.8$ Hz)

tons. The resonance at 1.59 ppm had been assigned to the **H′**3 protons of the acyl chain [10]. This assignment was confirmed by the correlation observed in the COSY spectrum. In addition, a second correlation was observed in this spectral region at 50°C: just upfield from the **H′**3 resonance at 1.59 ppm, two bands at 1.33 and 1.49 ppm were found to correlate to the **H**3 resonance which, in turn, exhibited a correlation to the **H**2 resonance at 3.88 ppm. Consequently, the peaks at 1.33 and 1.49 ppm were assigned to the two **H**4 protons of sphinganine. In the 1D proton spectrum, the peaks associated with protons **H′**3 and **H**4 were not completely resolved but their integration was about 4. The ^{1}H–^{13}C HMQC spectrum further confirmed these assignments as the two separate **H**4 proton bands were correlated to one single carbon resonance at 34.0 ppm corresponding to the **C**4 carbon of sphinganine.

As discussed in [10,11], the major differences in the proton resonances for DHSM and SM, with the critical double bond between carbons 4 and 5, are the absence of the vinylic proton resonances, seen at 5.45 and 5.7 ppm for **H**4 and **H**5 of SM, respectively, and the difference in chemical shift for **H**3. In SM, this proton exhibits a resonance at about 4.1 ppm, whereas in DHSM, this resonance is observed between 3.5 and 3.6 ppm, depending on the temperature and concentration of the sample. The upfield shift of this resonance in DHSM as compared to SM is to be expected, as the absence of the unsaturation site between carbons 4 and 5 results in greater shielding of proton **H**3 in DHSM.

3.2. ^{13}C spectral assignments

As the ^{13}C spectrum of DHSM had not been previously investigated, the assignments of ^{13}C resonances were sought. Since the ^{13}C NMR spectra at temperatures below 35°C were of poor S/N, the assignments listed in Table 2 correspond to the carbon resonances observed at 50°C. These assignments were obtained by analyzing the correlations observed in the ^{1}H–^{13}C HMQC spectrum and by comparison with assignments reported for similar lipids [50–53]. Once all of the proton resonances were clearly assigned, the ^{1}H–^{13}C correlations in the HMQC spectrum led to the assignment of the carbon peaks in a fairly straightforward fashion. With the exception of the resonances for the acyl chain carbons, only two resonances at 54.4 ppm were not completely resolved in the 1D ^{13}C spectrum. Their assignments were based on the correlations observed in the ^{1}H–^{13}C HMQC spectrum in which two cross peaks were seen for the 54.4 ppm resonance. One of them correlated with the ^{1}H resonance peak at 3.25 ppm assigned to the nine protons in three methyl groups of the choline group. The second correlation linked with the ^{1}H resonance at 3.88 ppm, which corre-

Table 2
Spectral assignment of ^{13}C NMR resonances observed for 80 mM DHSM in $CDCl_3$ at 50°C

Chemical shift (ppm)	Assignment	Reported value for sphinganine [50,51]
13.9	**C**H_3 (terminal methyl) [**C**18 of sphinganine chain and **C**′*n* of acyl chain[a]]	14.0 [50]
22.6	**C**17	22.5 [50]
	C′(*n*−1)[a]	
26.0	**C**5	23–24 [50]
26.1	**C**′3	
29.6	**C**H_2 (intermediate methylenes hydrophobic chains)	28.8–29.7 [40]
31.8	**C**16	31.9 [50]
	C′(*n*−2)[a]	
34.0	**C**4	
36.8	**C**′2	
54.4	**C**2	50–51 [50]
	N^+(**C**H_3)$_3$	54.5 [51]
59.3	**C**″1	59.9 [51]
65.2	**C**1	63 [50]
66.4	**C**″2	66.5 [51]
70.7	**C**3	69.4 [50]
173.4	O=**C**-NH	

[a]The acyl chain composition of the DHSM sample is not homogeneous. The main components correspond to saturated $C_{18:0}$ (34%) and $C_{24:0}$ (33%) acyl chains. No double bonds are present as they have been saturated during the hydrogenation reaction used to obtain DHSM from SM.

sponds to **H**2. Therefore, these overlapped resonances at 54.4 ppm correspond to the carbons of the three methyl groups of the choline head group and to **C**2, the second carbon of sphinganine. The resonance at 70.7 ppm was assigned to **C**3. As expected, this chemical shift differs from that for the **C**3 resonance in SM reported as 73.4 ppm [50], because of the absence of the double bond between **C**4 and **C**5 in DHSM. The resonances at 31.8 and 22.6 ppm were assigned to **C**16 and **C**17 of the sphingoid base, respectively. These assignments were based on previously published reports [50–53] in which the well established α, β and γ effects on ^{13}C chemical shifts were taken into consideration [51].

3.3. Concentration- and temperature-dependent conformational studies

This section describes the trends observed for ^1H and ^{31}P NMR spectral features as the temperature and concentration of partially hydrated (between two and three bound water molecules per phospholipid) and dehydrated (less than one bound water molecule per phospholipid) DHSM samples prepared in $CDCl_3$ were varied. For samples with concentrations higher than 13 mM and at temperatures below 35°C, most resonances became severely broadened due to the gelation of the lipid matrix. All concentration-dependent graphs are plotted as a function of DHSM concentration. A logarithmic scale was used for the concentration to emphasize the changes that take place at the lower concentrations, where the samples begin the formation of reverse micelles, as discussed in the next section. The error bars represent the S.D.s of three independent runs. In general, all proton resonances exhibited relative S.D. of 0.6% or less, except for the N**H** resonance, for which the maximal %R.S.D. was 1.0% for the partially hydrated samples (0.5% for dehydrated samples) over the temperatures and concentrations measured. The smooth curves are plotted to aid the visualization of the trends.

3.3.1. Head group region

Fig. 2 illustrates some of the major *concentration-dependent trends* observed in resonances corresponding to the interface and head group regions of partially hydrated DHSM samples in $CDCl_3$ at 50°C. The general trend exhibited by the head group resonances labeled **H**″1A and B, **H**″2 and choline methyl

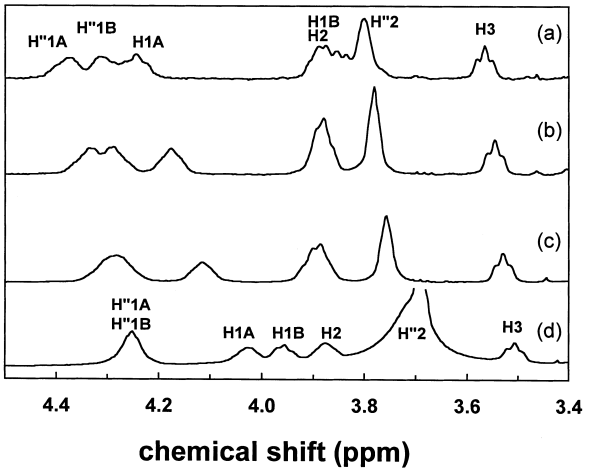

Fig. 2. Changes in ^{1}H NMR spectral resonances corresponding to the head group and interface regions of partially hydrated DHSM as a function of concentration in $CDCl_3$ at 50°C. (a) 8.4 mM; (b) 17 mM; (c) 24 mM and (d) 80 mM.

protons (not shown) was an upfield shift as the concentration was increased from 8.4 (a) to 80 mM (d). The changes in the resonances for **H″**1A and B were among the most pronounced and are graphed in Fig. 3 over the entire concentration range investigated for both the partially hydrated (solid symbols, solid lines) and dehydrated (open symbols, dotted lines) samples at 50°C.

The concentration-dependent changes observed for

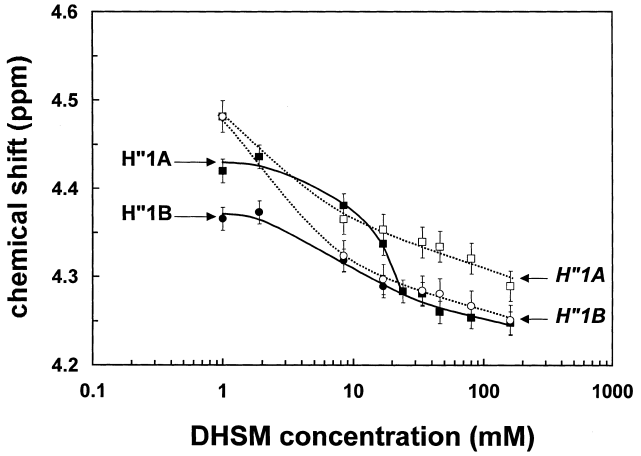

Fig. 3. Concentration dependence of the resonances corresponding to protons **H″**1A and B of the choline moiety at 50°C. Solid symbols and solid lines correspond to partially hydrated samples in $CDCl_3$. Open symbols and dotted lines correspond to dehydrated samples in $CDCl_3$. The error bars represent the S.D. of the chemical shifts obtained for three independent runs.

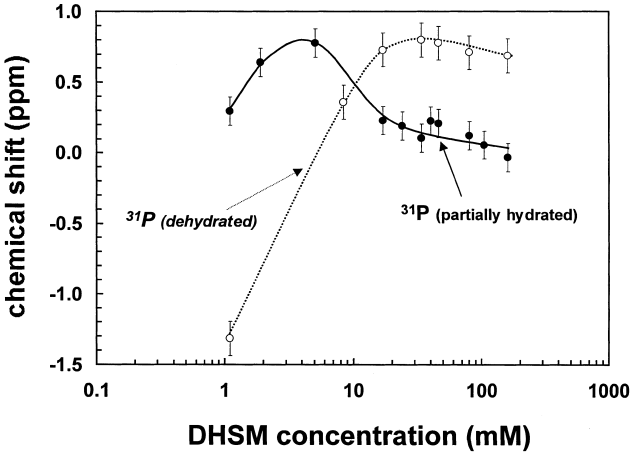

Fig. 4. Concentration dependence of the ^{31}P resonance corresponding to the phosphate head group at 50°C. Solid symbols and solid lines correspond to partially hydrated samples in $CDCl_3$. Open symbols and dotted lines correspond to dehydrated samples in $CDCl_3$. The error bars represent the S.D. of the chemical shifts obtained for three independent runs.

the ^{31}P resonance are shown in Fig. 4 for the partially hydrated (solid symbols, solid lines) and dehydrated samples (open symbols, dotted lines) samples at 50°C. The maximal S.D. in these measurements at 50°C was 0.10 ppm. All chemical shifts are referenced to 85% H_3PO_4.

The *temperature-dependent* trends seen in the head group proton resonances **H″**1A and B, **H″**2 and $N^{+}(C\mathbf{H}_3)_3$ were similar above 37°C. As the temperature was increased from 37 to 50°C, all these resonances exhibited a small increase (0.022 ± 0.004 ppm) in their chemical shift, indicative of a slight deshielding of the protons in the choline moiety. This trend with increasing temperature is similar in nature, but relatively smaller in magnitude, to that observed when diluting the sample. Below 35°C, the resonances were too broad (not shown) and their integration was no longer quantitative, suggesting a decrease in the transverse relaxation time T_2 when the temperature was lowered and the molecules interacted with each other more strongly, as would be the case in a gel state.

3.3.2. Interfacial region

Significant changes were observed with concentration and temperature in most of the resonances associated with the backbone or interfacial region of DHSM. Beginning with the resonances for the gemi-

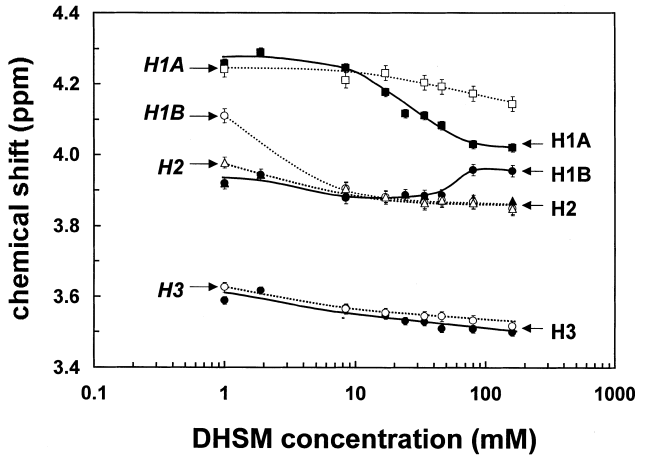

Fig. 5. Concentration dependence of the resonances corresponding to protons **H**1A and B, **H**2 and **H**3 of the interface region at 50°C. Solid symbols and solid lines correspond to partially hydrated samples in $CDCl_3$. Open symbols and dotted lines correspond to dehydrated samples in $CDCl_3$. The error bars represent the S.D. of the chemical shifts obtained for three independent runs.

nal, chemically nonequivalent protons **H**1A and B, Fig. 5 illustrates the interesting concentration dependence of their chemical shifts for partially hydrated (solid symbols, solid lines) and dehydrated (open symbols, dotted lines) samples. The **H**3 resonance in the partially hydrated samples followed the same concentration-dependent trend seen for the **H**1A resonance, although the magnitude was smaller.

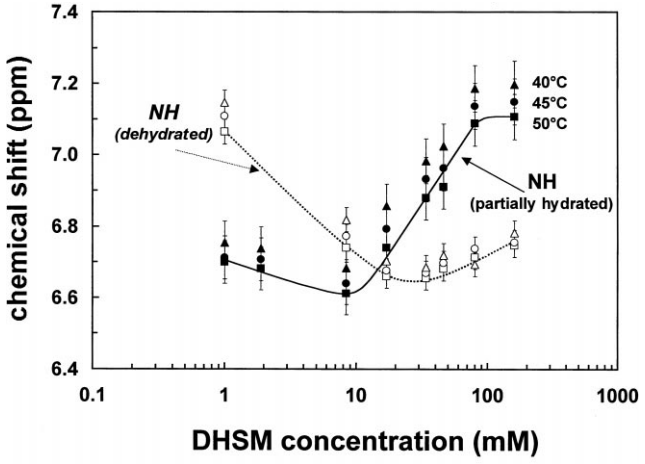

Fig. 6. Concentration dependence of the resonance corresponding to N**H** proton of the interface. Three temperatures are plotted for both partially hydrated (solid symbols and solid lines) and dehydrated (open symbols and dotted lines) samples in $CDCl_3$.

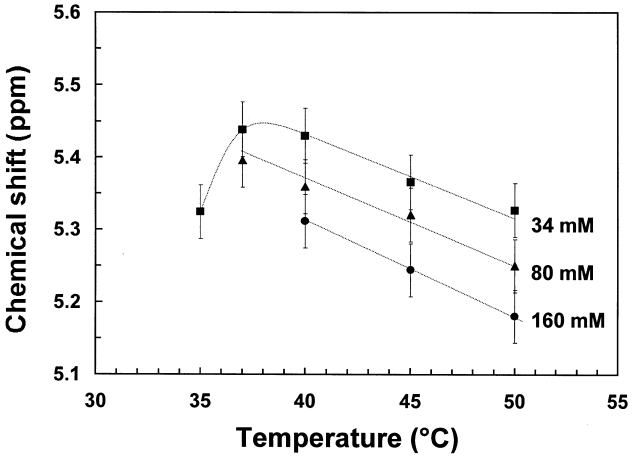

Fig. 7. Temperature dependence of the resonance corresponding to O**H** proton of the interfacial region of partially hydrated samples in $CDCl_3$. This broad resonance could hardly be detected at concentrations lower than 30 mM.

The concentration and temperature dependences of the N**H** and O**H** resonances are shown in Figs. 6 and 7, respectively. As seen in Fig. 6, for concentrations above 10 mM, the N**H** resonance of the partially hydrated samples shifted downfield as the concentration was increased up to about 80 mM. Beyond this concentration, no significant changes were observed. Quite a different trend was observed with the removal of water: at the lowest concentrations, the chemical shift of the N**H** resonance was 7.14 ± 0.08 ppm. A significant lowering in chemical shift occurred around 2–3 mM and then relatively small changes were seen for the higher concentrations. The rates of change in chemical shift δ with temperature T ($\Delta\delta/\Delta T$) were similar for the partially hydrated samples with concentrations above 13 mM. The average value for $\Delta\delta/\Delta T$ for the 17, 34, 80 and 160 mM samples was $-(8.9 \pm 0.7) \times 10^{-3}$ ppm/°C. This rate decreased to $-(6.4 \pm 0.2) \times 10^{-3}$ ppm/°C for the 1.9 and 1 mM samples.

3.3.3. Bound water resonance

The resonance observed for the water protons in the partially hydrated samples at the higher concentrations was fairly broad, particularly as the temperature was decreased and the concentration increased. The integration of this resonance varied between four and six protons. The concentration dependence of the chemical shift is shown in Fig. 8 at three temperatures, 40, 45 and 50°C. The solid curve rep-

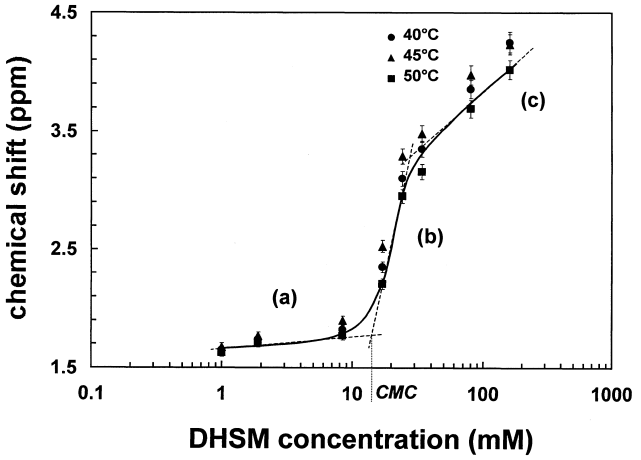

Fig. 8. Concentration dependence of the resonance corresponding to $\mathbf{H_2O}$ protons of the water molecules bound to DHSM. The CMC of DHSM in $CDCl_3$ was estimated to be 13 mM from the intercept of the two straight lines (a) and (b).

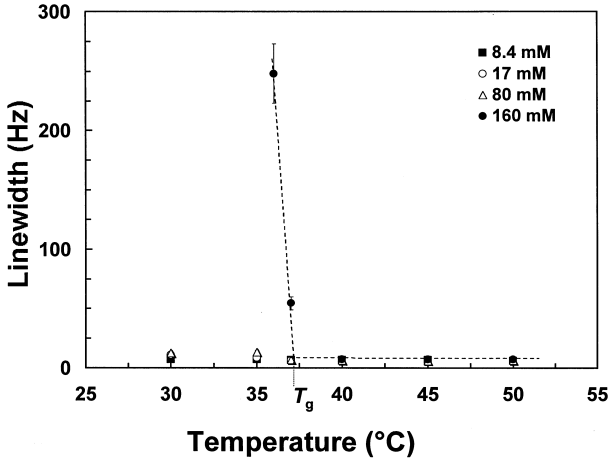

Fig. 9. Temperature dependence of the linewidth at half height of the $\mathbf{CH_2}$ resonance of the hydrophobic chains at different concentrations of partially hydrated DHSM in $CDCl_3$.

resents the trend followed at 50°C. The relationship between changes in the chemical shift of water and the molar concentration of the lipid has been used by other researchers to estimate the critical micelle concentration (CMC) [52,53]. As shown in Fig. 8, three straight lines can be discerned in the relationship between $\delta\,\mathbf{H_2O}$ and the logarithm of the molar concentration of DHSM. Lines (a) and (b) intercept at (13 ± 2) mM, whereas lines (b) and (c) intercept at (30 ± 3) mM. The slopes of the lines (b) and (c) correspond to the change of chemical shift (in ppm) per unit change in the logarithm of the concentration of DHSM (in mM) and were evaluated to be 5.02 ± 0.07 and 1.26 ± 0.11, respectively.

3.3.4. Hydrophobic chain region

As shown in Fig. 9, a significant increase in linewidth was observed for the $\mathbf{CH_2}$ resonances of the hydrocarbon chains as the temperature was lowered and the the hydrophobic chains of neighboring micelles became entangled. A definite change could also be observed visually, as the thick gel formed below the transition temperature changed into a more clear and fluid solution at higher temperatures. The temperature at which this significant increase in linewidth occurred was concentration-dependent and changed from 35°C at 80 mM to 37°C at 160 mM. For concentrations below 13 mM, no significant change could be observed, suggesting that most of the molecules were in either small aggregates and/or monomeric arrangements. At the higher concentrations, the magnitude of the increase in linewidth increased, indicative of a greater reduction in T_2.

An interesting resonance that reveals the effect of aggregation on the acyl chain is that corresponding to $\mathbf{H'}2$ protons, shown in Fig. 10 for three concen-

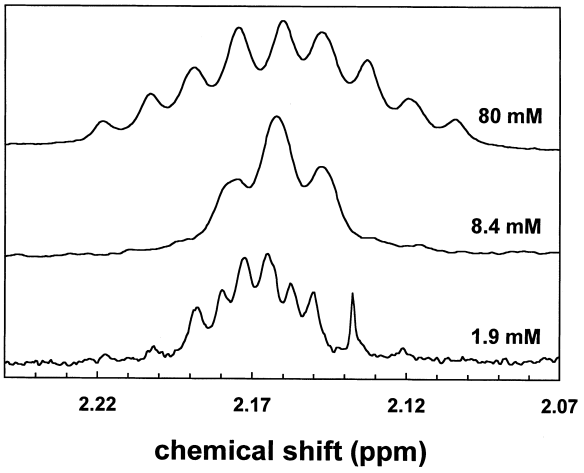

Fig. 10. Changes in the contour of the resonances for the $\mathbf{H'}2$ protons with concentration at 50°C. At the higher concentration (80 mM in $CDCl_3$), the protons become more distinct as the packing is tighter. This profile may reflect the overlap of two sextets, each of which results from the splitting of the $\mathbf{H'}2$ protons with each other and the H′3 protons. At the lowest concentration (1.9 mM in $CDCl_3$), a sextet is seen. At an intermediate concentration (8.4 mM in $CDCl_3$) the splitting pattern is less defined.

trations. At the intermediate concentration of 8.4 mM, this resonance exhibited a triplet-splitting pattern consistent with the splitting by equivalent **H′**3 neighboring protons. At the lowest concentrations, the profile resembled a sextet or octet. At the higher concentrations, the splitting pattern changed to an apparent decaplet. It is proposed that a conformational transition occurs in going from the monomeric to the aggregated form in which the two protons **H′**2A and B are affected by different levels of restriction into nonequivalent environments. The observed pattern at the higher concentrations could result from the partial overlap of two sextets (or higher multiplicity) corresponding to the splitting of each of the **H′**2 protons by each other and the **H′**3 protons.

3.4. Effect of hydration

The impact of hydration is seen in Fig. 11a,b for two concentrations at 50°C. The comparison of the top traces (Fig. 11a) obtained for the 8.4 mM sample of DHSM partially hydrated with two to three water molecules per phospholipid (solid line) and hydrated samples with at least 50 water molecules per phospholipid (dotted line) indicate several significant changes in the conformation of the head group and interface region: the resonances associated with the choline, **H″**1A and B, **H2″**, and choline methyl protons (not shown) shifted upfield when water was added. In particular, **H″**1A and B resonances, which appeared as two partially overlapped bands in the partially hydrated sample in $CDCl_3$, coalesced into one.

An upfield shift of the ^{31}P resonance was observed upon hydration (not shown). Indeed, upon hydration of all samples with concentrations above 3 mM, the ^{31}P chemical shift moved upfield to -0.06 ± 0.02 ppm. The hydration of the lowest concentrations, below 3 mM, resulted in an even greater upfield shift, moving the ^{31}P resonance to -0.28 ± 0.04 ppm.

The differences in the lower traces obtained before and after the addition of excess water to the 80 mM sample were less pronounced than those seen for the

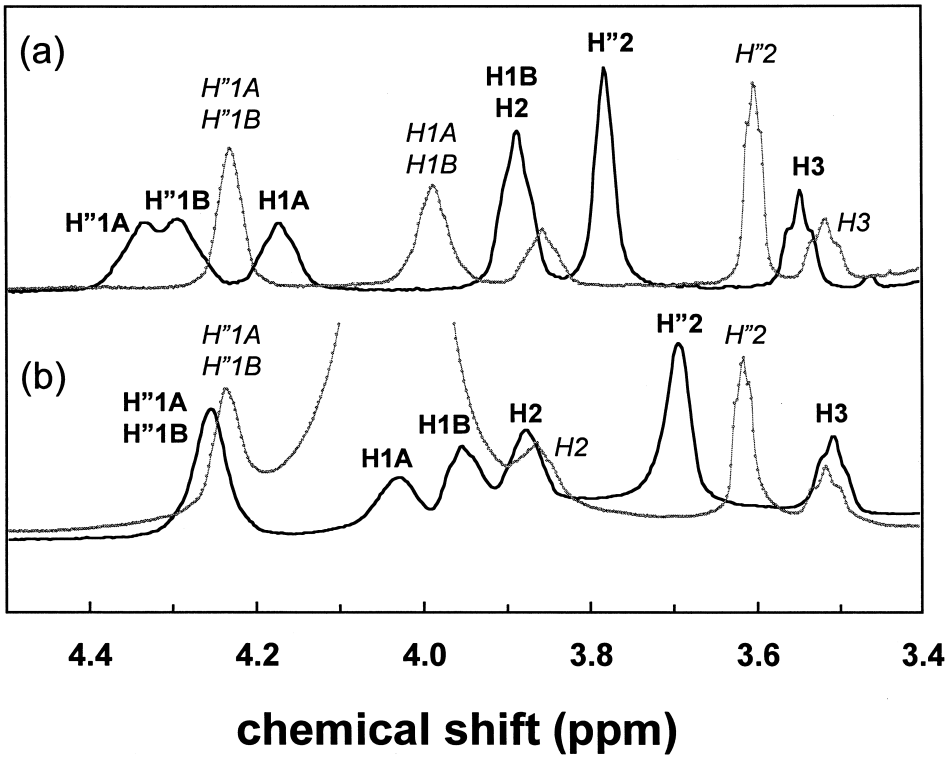

Fig. 11. Effect of hydration on the ^1H NMR spectral region corresponding to most of the head group and interface protons for two concentrations at 50°C: (a) 8.4 mM in $CDCl_3$ and (b) 80 mM. Solid lines represent the partially hydrated samples in $CDCl_3$. Gray lines show the spectral traces obtained after addition of excess water.

8.4 mM sample. Overall, the choline proton resonances did shift upfield but less than 0.1 ppm. For both concentrations, the choline proton resonances reached the same chemical shifts upon hydration. The **H**1A and B resonances were already fairly close in the partially hydrated sample. Their difference was (0.08 ± 0.01) ppm and, unfortunately, the final changes upon hydration could not be seen as these bands overlapped with the **H**DO resonance. At 35°C, however, the **H**DO band did not overlap the **H**1A and B resonances, which appeared within 0.03 ppm of each other. As in the lower concentration sample, the N**H** resonance shifted to 7.4 ± 0.1 ppm upon addition of water.

4. Discussion

The complex behavior observed in the self assembly of different phospholipids is the theme of intensive research and interest [54]. Sphingolipids, because of their approximately cylindrical shape and amphipathicity, exhibit a great tendency to form bilayer structures in aqueous media [1,2]. Recent reports [40–44], however, demonstrate the segregation of sphingolipids and cholesterol in the form of buoyant clusters (rafts) and caveolae and thus suggest that conventional bilayers are not the exclusive arrangement adopted by sphingolipids in membranes. One of the aims of this work was to characterize the conformational features of DHSM at different levels of aggregation and to establish the nature of lipid–lipid and lipid–water interactions. Although solid state NMR spectroscopy can been applied to the study of aggregated sphingolipids [27], high resolution NMR spectroscopy of phospholipids in aqueous media is limited as the lipids associate readily into liposomes. This results in the severe broadening of most of the resonance peaks due to both the decrease in the transverse-relaxation time T_2 and the increase in anisotropy [48]. As a consequence, it is not possible to assess either the changes that occur as the liposomes are formed or the final conformations adopted by the lipids in the hydrated vesicle. The lower polarity of chloroform, on the other hand, allows the monitoring of spectral changes that take place as the lipids go from a monomeric form, at very low concentrations, to an aggregated state at higher concentrations. At these higher concentrations reverse micelles are formed due to the interaction of the interface and head group regions of neighboring molecules. Although some broadening occurs, it is still possible to detect changes in spectral features. Excessive broadening only takes place when the micelles come into close proximity and enhanced van der Waals interactions cause the gelation of the sample.

This discussion deals with the average conformational preferences exhibited by DHSM over a wide range of concentrations in $CDCl_3$ and in different levels of hydration. Although it may be argued that the analysis of partially hydrated and dehydrated samples is of limited biological relevance, the information gained from these studies allows us to characterize the way in which strongly bound water molecules interact with the lipids and participate in the establishment of intricate H-bonding networks. The impact of these water molecules on the conformational arrangement of the lipids is of paramount relevance since water does not serve as a simple inert spectator, but is an essential component of biomembranes.

4.1. T_1 relaxation times and correlation times

To better understand the dynamics of the DHSM assemblies formed in chloroform, spin-lattice or longitudinal relaxation times T_1 were measured at two magnetic fields, 300 and 500 MHz, and at 50, 40 and 35°C for a 17 mM sample of partially hydrated DHSM in chloroform. At this concentration, as discussed later in this section, DHSM begins to form micelles. Furthermore, at this and higher concentrations, lowering the temperature below 35°C leads to the hydrophobic entanglement of neighboring micelles and thus to the gelation of the sample. This transition from a fluid to a gel state has been reported when minute amounts of water are added to phosphatidylcholine (PC) dissolved in highly non-polar solvents, such as isooctane and cyclohexane [55,56]. Interestingly, these organogels are not formed by PC in chloroform [57–63]. The values of T_1 measured at 300 MHz (not listed) were consistently lower than those at 500 MHz (listed in Table 3). From the values of T_1 at both fields, we were able to estimate the correlation time, τ_c, for the different

protons. The average values of τ_c were found to be between 0.55×10^{-10} (methylene protons) and 2.5×10^{-10} s (N**H**, **H**1A and B and **H**2) at 50°C. The average of all the τ_c values measured at 50°C for the proton resonances was $(1.5\pm0.6)\times10^{-10}$ s. At 40°C, the measured values of τ_c for most protons were within one S.D. of the values at 50°C, except for the methylene protons, for which the correlation time doubled. The overall average at 40°C was $(1.7\pm0.9)\times10^{-10}$ s. At 35°C, most bands were broadened significantly and the correlation times could not be determined accurately. However, from the decrease in T_1 as the temperature decreased and the proximity of τ_c to $1/\omega_0 = 1/2\pi500$ MHz = 3.2×10^{-10} s at the measured conditions, it is reasonable to expect that as the sample gels, due to either a decrease in temperature or an increase in the lipid concentration, the increase in viscosity η leads to an increase in τ_c ($\tau_c \propto 4\pi\eta$) [64]. The sample would then approach the condition at which $\tau_c \approx 1/\omega_0$. Beyond this point, T_1 is expected to increase and T_2 to decrease [48,64]. Under these conditions, the overall micelle reorientation may become the main mechanism by which the spin–spin relaxation is controlled. The reduction in T_2 leads to significant band broadening. Indeed, a significant increase of the linewidth in the C**H**$_2$ resonance was observed as the temperature of the sample decreased, particularly at the higher concentrations (Fig. 9). The temperature at which the C**H**$_2$ resonance linewidth increased dramatically and the sample became a gel will be denoted T_g and was estimated to be 37°C for the most concentrated (160 mM) sample in $CDCl_3$ (see Fig. 9). This temperature was even higher for the DHSM samples prepared in pure d-benzene (T_g = 47 ± 2°C) and in pure d-cyclohexane (T_g = 57 ± 2°C). These observations suggest that the micellar arrangement of DHSM in chloroform is more relaxed than that formed in the more nonpolar solvents. The actual shape of these DHSM micelles formed in chloroform is not known at this time, but the comparison of the trends presented herein with those reported for organogels of PC in cyclohexane and benzene [56] suggests a rod-like cylindrical shape for the reverse micelles formed in chloroform and a spherical, tighter geometry for those formed in the more nonpolar solvents, benzene and cyclohexane.

The presence of reverse micelles for temperatures above T_g is supported by the T_1 values measured in $CDCl_3$ and listed in Table 3. With the exception of the most concentrated sample at 37°C, the T_1 values for the protons in the terminal methyl and methylene groups of the hydrophobic chains were always significantly higher than the choline methyl protons of the head group. This trend is comparable to that reported for dipalmitoyl phosphatidylcholine (DPPC) in $CDCl_3$ and attributed by Lee et al. [57] to the formation of reverse micelles in which the choline methyl groups pack in the center of the micelle and the hydrophobic chains are relatively free. It is interesting to note that for the highly concentrated (160 mM) DHSM sample near the gel to fluid transition temperature of 37°C, the T_1 values for the methylene and terminal-methyl protons were of similar magnitude and significantly smaller than those measured at the lower concentrations for all temperatures (see Table 3). The overall trend suggests that at the higher concentrations of DHSM in $CDCl_3$, the reverse micelles come into close proximity and, due to the motional restriction caused by the entanglement of their hydrophobic chains, the T_1 values for the C**H**$_2$ and C**H**$_3$ resonances are reduced.

In pure D_2O, DHSM forms multilamellar liposomes or vesicles. The values of T_1 for the choline-methyl, methylene and terminal-methyl protons could not be measured below 50°C due to excessive

Table 3
T_1 values measured at 500 MHz for DHSM at various concentrations and temperatures (average ± S.D. of two independent determinations)

	$CDCl_3$, 17 mM, 50°C	$CDCl_3$, 17 mM, 40°C	$CDCl_3$, 17 mM, 35°C	$CDCl_3$, 160 mM, 37°C	D_2O, 34 mM, 50°C
Choline C**H**$_3$ (head group)	0.34 ± 0.01 s	0.31 ± 0.01 s	0.32 ± 0.02 s	0.51 ± 0.08 s	0.48 ± 0.01 s
C**H**$_2$ (hydrophobic chains)	1.2 ± 0.2 s	1.13 ± 0.07 s	0.98 ± 0.02 s	0.62 ± 0.09 s	0.85 ± 0.01 s
Terminal C**H**$_3$ (hydrophobic chains)	4.1 ± 0.8 s	3.2 ± 0.6 s	1.35 ± 0.11 s	0.68 ± 0.06 s	0.83 ± 0.21 s

broadening of the resonance bands. At 50°C, however, the T_1 values for methylene and terminal methyl protons in the choline and hydrophobic chains were of similar magnitude (Table 3). This trend compares well with that reported for PC in aqueous solution [57], in which multilayer vesicles or liposomes are formed. In addition, the comparable magnitude of the T_1 values measured for DHSM in the gel phase in $CDCl_3$ and in multilayer vesicles in D_2O, suggests that the dynamics of the gel state at high DHSM concentrations approximate those of a multilayer arrangement. This could result from the flattening and stacking of neighboring micelles as the hydrophobic tails begin to interdigitate and van der Waals interactions are maximized.

4.2. Monomer to reverse micelle transition

The CMC of partially hydrated DHSM was estimated to be 13 mM at 50°C from the dependence of the water resonance with concentration (see Fig. 8) and the changes in the chemical shifts of resonances associated with protons in the head group (Figs. 3 and 4) and the interface region (Figs. 5 and 6). In addition, the significant changes observed, particularly in the N**H** and ^{31}P resonances at concentrations below 3 mM, suggest that the average conformational arrangement of the interface and head group regions of DHSM differs at high levels of dilution. It is therefore proposed that DHSM exists as a monomer at concentrations below 3 mM. Between 3 and 13 mM, small aggregates may coexist with monomers. At concentrations above 13 mM, the strength of lipid–lipid and lipid–water interactions increases as the lipid molecules come closer to each other to form reverse micelles. From the concentration dependence of the N**H** resonance in the partially hydrated samples (Fig. 6), it appears that the interfacial regions of neighboring molecules have reached their maximal interaction around 80 mM for no further changes were seen in any of the interface resonances beyond this concentration.

The spectral features indicate that conformational changes do take place as the lipid molecules go from a solvated monomeric arrangement to an aggregated assembly held by lipid–lipid and lipid–water interactions. The discussion below addresses the nature of these average arrangements.

4.3. Conformational preferences of DHSM

The conformational arrangements discussed herein result from the concerted analysis of the trends presented in Section 3. It is important to note that due to the relatively long time scale (10^{-4} to 10^{-1} s) of the NMR experiment and the flexibility of these lipids, several conformers may be present at any one time. Therefore, the spectral features are representative of average conformational preferences. The discussion below leads to the postulation of several conformational arrangements of the head group and interfacial region of DHSM. The predominance of each conformer is affected by the state of aggregation and degree of hydration, as suggested below.

4.3.1. Partially hydrated DHSM, aggregated state

For concentrations above 13 mM, the N**H** resonance of the partially hydrated samples moved downfield, indicating of a deshielding of the N**H** proton as the concentration increased (Fig. 6). The relatively high values of $\Delta\delta/\Delta T$, the deshielding of the N**H** proton at higher concentrations and the marked lowering of the N**H** chemical shift upon removal of water (Fig. 6) suggest that, at the higher concentrations of partially hydrated DHSM, the average amide proton is mostly involved in intermolecular H-bonds with bridging water molecules. These H-bonds to water result in the greater deshielding of the N**H** proton and the strength of these bonds increases as lipids come into closer proximity. Because the amide proton is more involved in inter- rather than intramolecular H-bonds as the concentration is increased, the difference between the **H**1A and **H**1B resonances is reduced at the higher concentrations (Fig. 5). At concentrations below the CMC of partially hydrated DHSM, the two resonances differed by about 0.37 ± 0.01 ppm; this difference decreased with increasing concentrations up to ca. 80 mM. Beyond this concentration, the resonances maintained their difference of about 0.1 ppm. Contrasting these trends, the **H**1A and B resonances for the dehydrated samples above 13 mM differed by 0.35 ± 0.10 ppm and maintained this separation even at the higher concentrations. These trends in the interface proton resonances suggest that the internal restrictions that affect the partially hydrated samples at the lower concentrations and that place

H1A and B into fairly dissimilar magnetic environments are partially removed at higher concentrations. In comparable studies with PC carried out by others [57–63] and confirmed in our laboratory, the resonances for the corresponding geminal protons **H**1A and **H**1B on the glycerol backbone either overlapped (PC in $CDCl_3$) or differed by 0.01 ppm (PC in D_2O and PC in CD_3OD). The most obvious difference between DHSM and PC is the presence of H-bond donor sites (N**H** and O**H**) in the interfacial region of the sphingolipid. It is then proposed that as the concentration is increased and the interfaces of neighboring molecules approach each other, some of the intramolecular bonds involving the NH moiety are broken to form new intermolecular interactions.

Above the CMC, the ^{31}P chemical shift of the phosphate head group of partially hydrated DHSM exhibited an upfield shift (Fig. 4). This decrease in chemical shift can be related to a change from a *trans–gauche*, *gauche–trans* or *trans–trans* arrangement of the C1-O1-P-O″1 and O1-P-O″1-C″1 diester torsional angles (see Scheme 1) at the lower concentrations, in which the phosphate group is restricted by intramolecular H-bonds, to a more energetically favored *gauche–gauche* arrangement [65,66], in which the internal restrictions have been partially removed. Following this trend, the resonances corresponding to **H**″1A and B, which were distinct for the partially hydrated samples below 13 mM, coalesced into a single band. This suggests that as the DHSM molecules begin to interact and assemble into reverse micelles, the intramolecular restrictions that renders **H**″1A and B into dissimilar magnetic environments and the phosphate diester angles into a more *trans–gauche* or *gauche–trans* arrangement are disrupted.

The predominant arrangement proposed for DHSM in the aggregated state in the presence of bound water molecules is illustrated in Scheme 1. In this scheme, the amide proton is mainly involved in intermolecular H-bonds with water molecules that may act as bridges between the interfacial regions of neighboring DHSM molecules. It is also possible that at high concentrations, the OH group may mainly bond to neighboring lipids directly or through water bridges. The O**H** resonance, when detectable, was extremely broad in both partially hydrated or dehydrated samples. This could be due to a rapid exchange of this proton, which would indicate

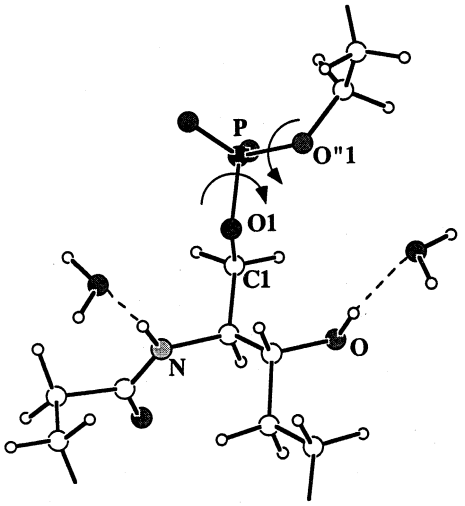

Scheme 1.

that this O**H** proton is fairly labile or involved in weak H-bonds. It is also possible that the **O**H group may act as an acceptor of H-bonds.

The O**H** resonance was detectable at the higher concentrations, 34 mM and above, but it was still very broad (between 100 and 150 Hz halfwidth). Although the precise determination of the chemical shift was difficult, an upfield shift was seen in going from 34 to 160 mM, as shown in Fig. 7. This suggests the shielding of the O**H** proton at the higher concentrations could be indicative of a weakening of an intramolecular H-bond when lipid–lipid or lipid–water interactions become prevalent. The $\Delta\delta/\Delta T$ was measured as $-(0.012 \pm 0.002)$ ppm/°C at these concentrations. This relatively high value points to the participation of this group in intermolecular H-bonds, possibly with water molecules. Interestingly, the role of this OH moiety is better defined in SM, in which the OH group is believed to be involved in a stronger intramolecular interactions, as discussed in [67].

The complex splitting pattern observed for the **H**′2 resonances at 80 mM (see Fig. 10) indicates the nonequivalence of the geminal protons **H**′2A and B in the aggregated state of DHSM. This could be due to the steric restrictions caused by the formation of H-bonds that bring the interfacial regions of neighboring molecules into close proximity.

4.3.2. Partially hydrated DHSM, nearly-monomeric and monomeric forms

The changes in the N**H** resonance at the lower concentrations suggest that rather than an intermolecular H-bond with water molecules, the NH moiety participates in an intramolecular H-bond. This possibility is supported by the difference in the temperature dependence of the N**H** chemical shift at these low concentrations. At the lowest concentrations, both a reversal in the concentration dependence of the chemical shift and a reduction to −0.006 ppm/°C in the rate of change $\Delta\delta/\Delta T$ between 37 and 50°C were observed (see Fig. 6). In addition, no significant difference was seen in the N**H** chemical shift for the two lowest concentrations investigated (1 and 2 mM, Fig. 6). Both the reduction in $\Delta\delta/\Delta T$ and the lack of change in δ with concentration suggest the participation of the N**H** moieties in intramolecular H-bonds [68]. As this bond is formed, the position of **H**1A and B into magnetically nonequivalent environments would lead to the observed significant difference in their chemical shifts (Fig. 5). The conformers that could lead to the trends observed below 13 mM are represented in Scheme 2a–c. In these schemes, the NH acts as a donor in the formation of intramolecular H-bonds that connect to the ester oxygen O″1 (Scheme 2a), or O1 (Scheme 2b), or an anionic phosphate oxygen (Scheme 2c) while the OH group interacts with an anionic phosphate oxygen (Scheme 2a,b) or the ester oxygen O1 (Scheme 2c).

The plausibility of these proposed schemes is validated by the results of molecular modeling studies carried out by molecular mechanics in our laboratory [69]. Although the molecule investigated in [69] had an abbreviated phosphodiester headgroup (methyl phosphoryl dihydroceramide), the conformational preferences of the interface region are in excellent agreement with the arrangements proposed in schemes above. The presence of intramolecular H-bonds in the proposed schemes affects the two diester torsional angles C1-O1-P-O″1 and O1-P-O″1-C″1 of the head group and is expected to favor a *trans–gauche* or *gauche–trans* arrangements for which the ^{31}P chemical shift is expected to be downfield (more positive chemical shift) as compared to a more energetically favored *gauche–gauche* configuration in the absence of intramolecular H-bonds [65]. This deshielding effect of the phosphorus nucleus is seen

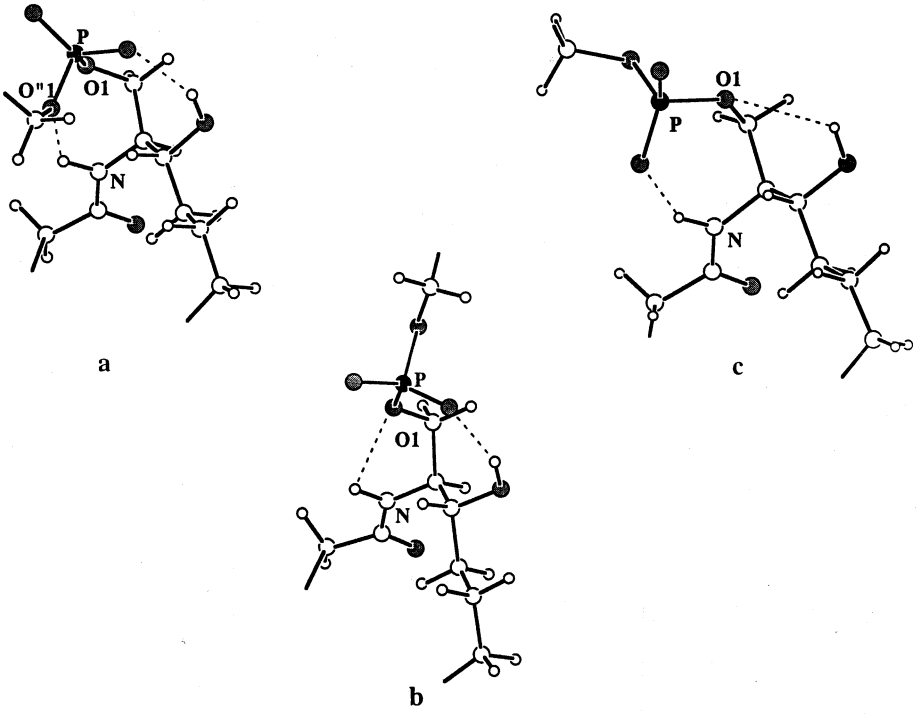

Scheme 2.

clearly as the concentration is lowered and the CMC is reached (see Fig. 4).

The complexity of the splitting pattern decreased for the **H**′2 resonances as the concentration was decreased from 80 to 8.4 mM (Fig. 10). This is attributed to the rupture of lipid–lipid interactions that restrict the motion of protons **H**′2A and B. At the lowest concentrations (below 3 mM), however, the splitting pattern became more complex. In addition, a slight downfield shift of the N**H** resonance accompanied by an upfield shift in the ^{31}P resonance were observed. These trends suggest the contribution, albeit minor, of a different monomeric arrangement in which the NH group may no longer restrict the orientation of the head group. This arrangement appears to prevail in the monomeric form of the dehydrated samples and is discussed in detail later in this section.

4.3.3. Dehydrated DHSM, aggregated form

The differences caused by removal of water on the arrangement of the interface and head group regions are demonstrated in Figs. 3–6. Although the conformational preferences of dehydrated phospholipids may be irrelevant to the organization of DHSM in biomembranes, their characterization helps in our assessment of the tremendous impact of water in the conformational features of DHSM. For concentrations above 13 mM, relatively little change was seen for the N**H** resonance of the dehydrated samples. In addition, the values of $\Delta\delta/\Delta T$ were quite small, $-(0.0036 \pm 0.0004)$ ppm/°C. These trends, the maintained difference in chemical shifts for the **H**1A and B (open symbols in Fig. 5) as well as **H**″1A and B resonances (open symbols in Fig. 3), the downfield chemical shift for the ^{31}P resonance and its lack of change above 13 mM (open symbols in Fig. 4) indicate that the same arrangements discussed for the nearly monomeric, partially hydrated samples prevails in the dehydrated samples at higher concentrations. In these arrangements, illustrated in Scheme 2a–c, the N**H** group is involved in intramolecular H-bonds in which ester and/or an anionic phosphate oxygens may act as acceptors. These observations suggest that in the absence of water, the N**H** of the amide group cannot be dislodged from its intramolecular bond to the phosphate head group.

4.3.4. Dehydrated DHSM, monomeric form

At the lowest concentrations of the dehydrated samples, the N**H** appears to be involved in a different type of intramolecular H-bond in which the acceptor is *not* in the head group. The arrangement illustrated in Scheme 3 could explain several trends observed at the lowest concentrations in the absence of water: the complete elimination of differences and downfield shift of the **H**″1A and B resonances (open symbols in Fig. 3), the large upfield shift in the ^{31}P resonance (open symbols in Fig. 4), the significant reduction in the difference of chemical shifts for **H**1A and B (open symbols in Fig. 5) and the sharp increase in the chemical shift for the N**H** resonance (open symbols in Fig. 6). Scheme 3 shows that the acceptor site may be the **O**H group of the sphinganine base, as suggested by the downfield shift seen in the **H**3 resonance of the dehydrated samples as compared to the partially hydrated samples (Fig. 5). Hartree–Fock ab initio calculations carried out at the 6-31G** level on a secondary alcohol indicate that there would be a reduction in the charge of **H**3 when the **O**H acts as an acceptor. Conversely, a shielding effect would be expected if the O**H** acted as a donor, since an increase in negative charge of **H**3 is found theoretically. In this scheme the phosphate group is not restricted by intramolecular H-bonds and the torsional diester angles C1-O1-P-O″1 and O1-P-O″1-C″1 would be expected to adopt the most favorable *gauche–gauche* conformation, with a corresponding upfield shift in the ^{31}P resonance. This effect is seen in the ^{31}P chemical shift for the dehy-

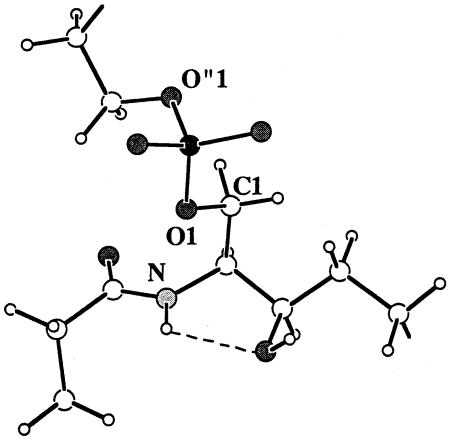

Scheme 3.

drated monomer, where the very upfield chemical shift observed ($\delta = -1.3$ ppm) is suggestive of an arrangement without intramolecular restrictions around the phosphate group.

4.4. Impact of hydration

Although the spectral changes observed upon addition of water were more pronounced for the 8.4 mM (Fig. 11a) than for the 80 mM sample (Fig. 11b), the nature of the changes was similar. In both cases, complete hydration resulted in a downfield shift of the N**H** resonance. This and the overlap of **H**1A and B resonances (Fig. 11a), which differed by about 0.3 ppm in the partially hydrated samples (Fig. 5) indicate the possible weakening or partial rupture of the intramolecular H-bond established between the N**H** group and the ester oxygen O1 or an anionic phosphate oxygen. The weakening of this bond as lipid–lipid interactions and lipid–water interactions become predominant, would reduce the restriction around the geminal protons **H**1A and B imposed by the intramolecular H-bond. The N**H** group, instead, would be then bonded to bridging water molecules that would extend the H-bonding network established around the interface regions of neighboring DHSM molecules.

This postulate is supported by the changes in the resonances associated with the headgroup. With the addition of excess water, the resonances corresponding to **H**″1A and B that were partially resolved in the 8.4 mM sample of partially hydrated DHSM, coalesced into a single band. The ^{31}P chemical shift moved upfield to $\delta = -0.06$ ppm for both concentrations. This is consistent with a weakening of the proposed intramolecular H-bonds that restrict the phosphate anion in the partially hydrated state, particularly at the lower concentrations. From all the changes, it is then inferred that in the hydrated samples intramolecular H-bonds are significantly displaced and allow for a less restricted arrangement of the phosphate group. The formation of intermolecular H-bonds involving water molecules and the amide and phosphate moieties prevails. Interestingly, the hydration of lipids at the lowest concentrations investigated resulted in a ^{31}P chemical shift of -0.28 ppm, further upfield than in any other hydrated sample. In this case, it is proposed that the presence of conformers without any internal restrictions, such as that represented in Scheme 3, allows for an even more extensive interaction between water molecules and the phosphate group.

5. Conclusions

Significant conformational differences between the monomeric and the aggregated arrangements of DHSM are evident from the analysis of the spectral data. The intramolecular H-bonds that prevail below the CMC are partially disrupted by the formation of intermolecular H-bonds between the amide proton and water. The impact of water in the aggregation process is indeed relevant and suggests that bridging water molecules are an integral part of the H-bonding network established among the interface regions of DHSM.

The comparison of these trends and those reported for SM in the accompanying report [67] point to the key role of the NH and OH groups in the nature of the intra- and intermolecular interactions. The NH moiety appears to be capable of participating in stronger intermolecular H-bonds in DHSM than in SM. These interactions connect neighboring lipids through water molecules. If the OH group is involved in a weaker intramolecular H-bond in DHSM as compared to SM, it could be more available or reachable, either as a donor or acceptor, for the formation of intermolecular H-bonds. This also would account for the higher transition temperature observed in DHSM as compared to SM and the differences in solubility of these lipids in chloroform: whereas SM dissolves readily, sonication and/or heating is required to dissolve DHSM.

At this time, the reasons behind the tendency of the OH and NH groups of DHSM to form weaker intramolecular H-bonds are being investigated in our laboratory using molecular modeling and experimental studies of fragments of these two lipids. It is expected that the conformational characterization of these enigmatic molecules will provide helpful information in unraveling their biological role(s) as components of biomembranes and as participants in cell signaling mechanisms.

Acknowledgements

We gratefully acknowledge the National Eye Institute of the National Institutes of Health, which has supported this research through grant EY11657 (M.C.Y.). Partial support was received by the National Computational Science Alliance under grants CHE98008N and CHE990012N for utilization of the NCSA HP/Convex Exemplar SPP-2200. We are indebted to Dr. Richard A. Porter for his helpful advice in the execution of NMR experiments.

References

[1] R.B. Gennis, in: Biomembranes: Molecular Structure and Function, Springer, New York, 1989, ch. 1.
[2] D. Voet, J.G. Voet, in: Biochemistry, Wiley, New York, 1995, ch. 11.
[3] L. Pick, M. Bielchowsky, Klin. Wochenschr. 6 (1927) 1631–1637.
[4] D. Shapiro, H.M. Flowers, J. Am. Chem. Soc. 84 (1962) 1047–1050.
[5] K.A. Karlsson, Chem. Phys. Lipids 5 (1970) 6–43.
[6] R.M. Broekhuyse, Biochim. Biophys. Acta 187 (1969) 354–365.
[7] G.L. Feldman, L.S. Feldman, G. Rouser, Lipids 1 (1966) 161.
[8] G.L. Feldman, T.W. Culp, L.S. Feldman, C.K. Grantham, H.T. Jonnson Jr., Invest. Ophthalmol. Vis. Sci. 3 (1964) 194–197.
[9] T.E. Merchant, J.H. Lass, P. Meneses, J.V. Greiner, T. Glonek, Invest. Ophthalmol. Vis. Sci. 32 (1991) 549–555.
[10] W.C. Byrdwell, D. Borchman, R.A. Porter, K.G. Taylor, M.C. Yappert, Invest. Ophthalmol. Vis. Sci. 35 (1994) 4333–4344.
[11] S.R. Ferguson, D. Borchman, M.C. Yappert, Invest. Ophthalmol. Vis. Sci. 37 (1996) 1703–1705.
[12] D. Borchman, W.C. Byrdwell, M.C. Yappert, Invest. Ophthalmol. Vis. Sci. 35 (1994) 3938–3943.
[13] J.V. Grenier, D.B. Auderbach, C.D. Leahy, T. Glonek, Invest. Ophthalmol. Vis. Sci. 35 (1994) 3739–3746.
[14] D. Shapiro, H.M. Flowers, S. Spector-Shefer, J. Am. Chem. Soc. 81 (1959) 3743–3749.
[15] L.J. Tirri, N.K.N. Ayengar, L.C. Lipton, N. Chatterjie, H. Brockerhoff, Lipids 13 (1978) 267–269.
[16] P.B. Schneider, E.P. Kennedy, J. Lipid Res. 9 (1968) 58–64.
[17] P.B. Schneider, E.P. Kennedy, J. Lipid Res. 8 (1967) 202.
[18] Y. Barenholz, T.E. Thompson, Biochim. Biophys. Acta 604 (1980) 129–158.
[19] W.I. Calhoun, G.G. Shipley, Biochim. Biophys. Acta 555 (1979) 436–441.
[20] P.R. Maulik, P.K. Spirada, G.G. Shipley, Biochim. Biophys. Acta 1062 (1991) 211–219.
[21] I. Pascher, Biochim. Biophys. Acta 455 (1976) 433–451.
[22] I. Pascher, S. Sundell, Chem. Phys. Lipids 20 (1977) 175–191.
[23] R.S. Khare, C.R. Worthington, Biochim. Biophys. Acta 514 (1978) 239–254.
[24] K.S. Bruzik, Biochim. Biophys. Acta 939 (1988) 315–326.
[25] C.F. Schmidt, Y. Barenholz, T.E. Thompson, Biochemistry 16 (1977) 2649–2656.
[26] D.J. Siminovitch, K.R. Jeffrey, Biochim. Biophys. Acta 645 (1991) 270–278.
[27] K.S. Bruzik, J.S. Harwood, J. Am. Chem. Soc. 119 (1997) 6629–6637.
[28] O.P. Lamba, D. Borchman, D.K. Sinha, S. Lal, M.C. Yappert, M.F. Lou, J. Mol. Struct. 248 (1991) 1–24.
[29] S.W. Hui, T.P. Stewart, P.L. Yeagle, Biochim. Biophys. Acta 601 (1980) 271–281.
[30] D. Borchman, W.C. Byrdwell, M.C. Yappert, Ophthalm. Res. 28 ((Suppl. 1)) (1996) 81–85.
[31] A.H. Merrill Jr., D.D. Jones, Biochim. Biophys. Acta 1044 (1990) 1–12.
[32] Y.A. Hannun, C.M. Linardic, Biochim. Biophys. Acta 1154 (1993) 223–236.
[33] Y.A. Hannun, J. Biol. Chem. 269 (1994) 3125–3128.
[34] Y.A. Hannun, R.M. Bell, Science 243 (1989) 500–507.
[35] A.H. Merrill Jr., V.L. Stevens, Biochim. Biophys. Acta 1010 (1989) 131–139.
[36] A.H. Merrill Jr., E.-M. Schmelz, D.L. Dillehay, S. Spiegel, J.A. Shayman, J.J. Schroeder, R.T. Riley, K.A. Voss, E. Wang, Toxicol. Appl. Pharmacol. 142 (1997) 208–225.
[37] S. Hakamori, J. Biol. Chem. 265 (1990) 18713–18736.
[38] L.K. Li, L. So, A. Spector, J. Lipid Res. 26 (1985) 600–609.
[39] L.K. Li, L. So, A. Spector, Biochim. Biophys. Acta 987 (1987) 112–120.
[40] K. Simons, E. Ikonen, Nature 387 (1997) 569–572.
[41] R.E. Brown, J. Cell Sci. 111 (1998) 1–9.
[42] N.M. Hooper, Mol. Membr. Biol. 16 (1999) 145–156.
[43] R.F. Jacobs, R.J. Cenedella, R.P. Mason, J. Biol. Chem. 274 (1999) 31613–31618.
[44] M.C. Yappert, X. Jin, D.B. DuPré, D. Tang, D. Borchman, Invest. Ophthalmol. Vis. Sci. 41 (2000) 4583.
[45] L. Braunschweiler, R.R. Ernst, J. Magn. Reson. 29 (1983) 521–528.
[46] D.G. Davis, A. Bax, J. Am. Chem. Soc. 107 (1985) 2820–2821.
[47] A. Bax, S. Subramanian, J. Magn. Reson. 67 (1986) 565–569.
[48] A.E. Derome, in: Modern NMR Techniques for Chemistry Research, Pergamon Press, Oxford, 1987, ch. 5.
[49] M. Sundaralingam, Ann. N. Y. Acad. Sci. 195 (1972) 324.
[50] W. Stoffel, O. Zierenberg, B.D. Tunggal, Hoppe-Seyler's Z. Physiol. Chem. 353 (1972) 1962–1969.
[51] E. Breitmaier, W. Voelter, in: Ebel, H.F. (Ed.), Carbon-13 NMR Spectroscopy: High Resolution Methods and Appli-

cations in Organic Chemistry and Biochemistry, 3rd edn., Weinheim, New York, 1987, pp. 183–186 and p. 467.
[52] Y.K. Levine, N.J.M. Birdsall, A.G. Lee, J.C. Metcalfe, Biochemistry 11 (1972) 1416–1421.
[53] J.F. Santaren, M. Rico, J. Guilleme, A. Ribera, Biochim. Biophys. Acta 687 (1982) 231–237.
[54] G. Cevc, Biochim. Biophys. Acta 1031 (1990) 311–382.
[55] D. Capitani, E. Rossi, A.L. Segre, Langmuir 9 (1993) 685–689.
[56] D. Capitani, A.L. Segre, F. Dreher, P. Walde, P.L. Luisi, J. Phys. Chem. 100 (1996) 15211–15217.
[57] A.G. Lee, J.M. Birdsall, Y.K. Levine, J.C. Metcalfe, Biochim. Biophys. Acta 255 (1972) 43–56.
[58] A. Kovac, J. Kidric, D. Hadzi, J. Mol. Struct. 267 (1992) 399–404.
[59] J. Kidric, J. Grdadolnik, A. Kovac, D. Hadzi, Stud. Biophys. 138 (1990) 51–55.
[60] W.R. Klemm, H.J. Williams, Alcohol 13 (1996) 133–138.
[61] H. Hauser, W. Guyer, I. Pascher, P. Skrabal, S. Sundell, Biochemistry 19 (1980) 366–373.
[62] G. Datta, P.S. Parvathanathan, U.R.K. Rao, K. Deniz, Physiol. Chem. Phys. NMR 24 (1992) 51–61.
[63] R. Hague, I.J. Tinsley, S. Schmedding, J. Biol. Chem. 247 (1972) 157–161.
[64] C.R. Cantor, P.R. Schimmel, in: Biophysical Chemistry, Part II: Techniques for the Study of Biological Structure and Function, W.H. Freeman, San Francisco, CA, 1980, pp. 497–506.
[65] D.G. Goldstein, in: Phosphorus-31 NMR, Principles and Applications, Academic Press, Orlando, FL, 1984, pp. 9–23.
[66] D. Perahia, B. Pullman, Biochim. Biophys. Acta 435 (1976) 282–289.
[67] C.M. Talbott, I. Vorobyov, D. Borchman, K.G. Taylor, D.B. DuPré, M.C. Yappert, Biochim. Biophys. Acta 1467 (2000) 326–337.
[68] S.H. Gellman, G.P. Dado, G.-B. Liang, B. Adams, J. Am. Chem. Soc. 113 (1991) 1164–1173.
[69] D.B. DuPré, M.C. Yappert, J. Mol. Struct. Theochem. 467 (1999) 115–133.